Bilayer ice and alternate liquid phases of confined water

Ronen Zangi and Alan E. Mark

Citation: The Journal of Chemical Physics **119**, 1694 (2003); doi: 10.1063/1.1580101
View online: http://dx.doi.org/10.1063/1.1580101
View Table of Contents: http://scitation.aip.org/content/aip/journal/jcp/119/3?ver=pdfcov
Published by the AIP Publishing

Bilayer ice and alternate liquid phases of confined water

Ronen Zangi[a] and Alan E. Mark[b]
The Groningen Biomolecular Sciences and Biotechnology Institute, Department of Biophysical Chemistry, University of Groningen, Nijenborgh 4, 9747 AG Groningen, The Netherlands

(Received 7 November 2002; accepted 15 April 2003)

We report results from molecular dynamics simulations of the freezing and melting, at ambient temperature ($T=300$ K), of a bilayer of liquid water induced by either changing the distance between two confining parallel walls at constant lateral pressure or by lateral compression at constant plate separation. Both transitions are found to be first order. The system studied consisted of 1200 water molecules that were described by the TIP5P model. The in-plane symmetry of the oxygen atoms in the ice bilayer was found to be rhombic with a distorted in-registry arrangement. Above and below the stability region of the ice bilayer we observed two bilayer phases of liquid water that differ in the local ordering at the level of the second shell of nearest neighbors and in the density profile normal to the plane, yielding two liquid phases with different densities. These results suggest the intriguing possibility of a liquid–liquid transition of water, confined to a bilayer, at regions where the ice bilayer is unstable with respect to either of the liquid phases. In addition, we find that under the same conditions, water confined to 3–8 layers remains in the liquid phase (albeit stratification of the transverse density profile) with values of the lateral diffusion coefficient comparable to that of the bulk. © *2003 American Institute of Physics.* [DOI: 10.1063/1.1580101]

I. INTRODUCTION

The behavior of materials under confinement, for example, between parallel plates only a few particle diameters apart, can exhibit a profound differences in properties (such as the viscosity of liquids or the symmetry of crystals) compared to those found in the bulk. In particular, confinement of many liquids to films less than 4–6 molecular layers will promote solidification.[1–10] This is due to the stratification of liquids against a wall that extends over 2–3 particle diameters. Such a layering phenomenon is enhanced when two walls confine the liquid to a narrow slit. In this case, the translation of the particles in the direction normal to the walls is restricted, which can induce lateral ordering and result in freezing. The degree to which the stability of the solid phase is enhanced depends on the ability of the particles to establish in-plane interparticle interactions.

Recently, it has been shown that the role of the local tetrahedral order of water is much more important than previously appreciated, especially in determining phase behavior and critical properties.[11] Computer simulations of supercooled bulk liquid water indicate the existence of a second critical point below which the liquid phase separates into two distinct phases: a low-density liquid (LDL) and a high-density liquid (HDL). It has been suggested that these two liquid water phases are closely related to the phases that exist at lower temperature, namely, low-density amorphous ice and high-density amorphous ice.[12,13] Recently, another study using restricted ensemble Monte Carlo method predicted the existence of four supercooled water liquid phases at $T=235$ K.[14] Experimental evidence for such a liquid–liquid transition in water is hard to obtain due to nucleation that occurs in that region of the phase diagram; however, liquid–liquid transition has been experimentally observed in fluid phosphorus.[15]

Monte Carlo studies of liquid water between two confining walls predicted a liquid–liquid transition between a bilayer of liquid water and a trilayer of liquid water at $T=235$ K.[16] Liquid water has also been the subject of computer simulations that explored the stability of water inside cylindrical nanopores and inside spherical cavities.[17–20] The first outer layer exhibited a distortion of the tetrahedral structure toward a square lattice arrangement.

In previous molecular dynamics (MD) simulation studies of a bilayer of liquid water with the TIP4P water model confined to a slab geometry, a freezing transition to a bilayer ice was reported.[21,22] However, the structures obtained in these calculations contained dramatic deviations from the molecular tetrahedral geometry around the oxygen atom. Hydrogen bonding interactions are insufficient to cause rehybridization of the sp^3 hybridized oxygen atom of water, which could results in a change in either the molecular H–O–H angle or in the spatial distribution of the electron lone pairs.[23,24] Therefore, it is expected that in confined geometries the tetrahedral molecular arrangement of the water molecules is preserved and the degree of the hydrogen bond distortion (from a collinear angle) would be in the range of the distortions found in the high-pressure bulk ice phases.

X-ray and neutron scattering studies of the structure of water in a hydrogel and at a hydrophobic surface observed that the first peak in the radial distribution function is not significantly affected due to the restricted geometries. However, a hump appears at around $r=0.37$ nm in a manner identical to that induced by a pressure increase and is interpreted in terms of the distortion of the hydrogen bonds.[25–27]

[a]Electronic mail: r.zangi@chem.rug.nl
[b]Electronic mail: a.e.mark@chem.rug.nl

In this study we investigate the phase behavior of water confined to 2–8 layers at ambient conditions. We find that a first-order freezing and melting of bilayer of liquid water can be induced by changing the distance between two confining parallel walls at constant lateral pressure or, alternatively, by lateral compression at constant plate separation. The in-plane symmetry of the oxygen atoms in the ice bilayer is rhombic, with a distorted in-registry arrangement. Above and below the region the ice bilayer is stable; we find two bilayer phases of liquid water that differ in the local ordering of the second shell of nearest neighbors and in the density profile along the normal direction. In addition, we find that under the same conditions, water confined to 3–8 layers remains in the liquid phase (albeit stratification of the transverse density profile) with values of the lateral diffusion coefficient comparable to that of the bulk.

II. METHODS

The MD simulations were performed using the GROMACS package version 3.0.[28] The time step used for integrating Newton's equations of motion was 0.002 ps. All simulations were performed using a constant number of particles and each system was coupled to a thermal bath[29] of $T=300$ K using a coupling time of 0.1 ps. In simulations where lateral pressure coupling[29] was employed, a coupling time of 1.0 ps was used. The value of the isothermal compressibility was set to either 1×10^{-5} or 5×10^{-7} bar^{-1}, depending on whether the phase was liquid or solid, respectively. The evaluation of the nonbonded interactions was performed using a twin range cutoff of 0.9 and 1.4 nm. Interactions within the shorter cutoff were updated every step, while longer range interactions were updated every five steps. To account for the neglect of electrostatic interactions beyond the long-range cutoff a reaction-field correction[30] assuming a relative dielectric constant of 78.0 was applied.

The five-site, tetrahedrally coordinated, TIP5P model[31] was used to describe the water molecules. A system of 1200 water molecules was placed between two walls with a triangular arrangement of atoms out of registry with respect to one another. The positions of the monolayer of atoms within the walls were constrained to a lattice spacing of 0.23 nm. The water–wall interactions were represented by a 6–12 Lennard-Jones (LJ) potential with the parameters: $\sigma_{(O_w-W)}=0.316$, $\sigma_{(H_w-W)}=0.284$ nm and $\epsilon_{(O_w-W)}=0.831$, $\epsilon_{(H_w-W)}=0.415$ kJ/mol. These parameters represent approximately the van der Waals (vdW) interaction between a water molecule and a quartz (SiO_2) surface. A weighted average of silicon and oxygen atom parameters, taken from the GROMOS96[32] force field, was used in a geometric combination rule together with TIP5P parameters. The simulations pertain, therefore, only to confinements due to surfaces where the interactions with the water molecules are weaker than hydrogen bonding interactions. Since the LJ parameters of the TIP5P water hydrogen are equal to zero, $\sigma_{(H_w-W)}$ was estimated from the ratio of the vdW radius between oxygen and hydrogen.[33] The value of $\epsilon_{(H_w-W)}$ was taken as half the corresponding value associated with oxygen. There was no interaction between the two lone-pair sites of water and the wall. There was no interaction between the lone-pair electrons sites and the surface atoms because the TIP5P lone-pair sites contain only electrostatic interactions (with LJ parameters equal to zero), while the surface atoms contain only LJ interactions. The same situation occurs with the hydrogen sites. However, since hydrogen atoms can be associated with a vdW volume we included an estimate of the potential between the surface atoms and the hydrogen atoms based on a measured value of the vdW radius for a hydrogen atom.[33]

The O–H bond lengths and the H–O–H bond angle were constrained using the SETTLE algorithm.[34] The lone-pair electrons were treated as dummy (virtual) atoms. Their positions are computed as a function of the oxygen and the hydrogens' positions. Then, the forces acting on the dummy atoms are distributed over the water atoms treated explicitly. In this way, the total energy and the total angular momentum of the system are conserved.[35]

The initial configuration in the first set of simulations (with lateral pressure coupling) was constructed from a previous simulation of a water bilayer in the liquid state.[36] At each thermodynamic point, obtained by a sequential increase in H, the system was equilibrated for 7 ns and then configurations saved every 10 ps for an additional 3 ns. At points where a phase transition occurred ($H=0.64$ and 0.70/0.72 nm), the equilibration time was extended to 17 ns to ensure convergence. The two series of simulations with different lateral pressure coupling were performed independently of each other after the preparation stage.

In the second set of the simulations (at constant A and H), a configuration corresponding to a bilayer in the liquid phase was taken from the first set of simulations. The area of the system was then increased or decreased in small incremental steps and simulated for time periods the same as those used in the first set of simulations.

The wall separation, H, was derived from the gap between the fixed center of mass of the surface atoms. These gap values were calibrated using the transverse distribution of the density of the center of mass of the oxygen atoms in a simulation corresponding to $H=0.58$ nm (which exhibited the sharpest distribution against the wall). To this value, the diameter of a water oxygen atom was added. The cutoff distance used to assign the presence of a hydrogen bond was taken as the distance to the minimum between the first and the second peaks of the oxygen–hydrogen pair correlation function in the different phases. This yielded a cutoff value of 0.232 nm.

III. RESULTS AND DISCUSSION

Figure 1 shows the lateral diffusion coefficient for plate separations in the range $0.57\ \text{nm}\leqslant H\leqslant 1.14\ \text{nm}$ for lateral pressures, P_l, of 1 and 100 bar. For plate separations in the range $0.57\ \text{nm}\leqslant H\leqslant 0.63\ \text{nm}$ the bilayer is in the liquid phase, as indicated by the large value of the diffusion coefficient which is comparable to the experimental value ($2.30\cdot10^{-5}$ cm^2/s) and to the TIP5P model value[37] ($2.62\cdot10^{-5}$ cm^2/s) for the bulk liquid water at $T=298$ K. At $H=0.64$ nm the lateral diffusion coefficient drops by about 3 orders of magnitude. At this point, the dynamics of the mol-

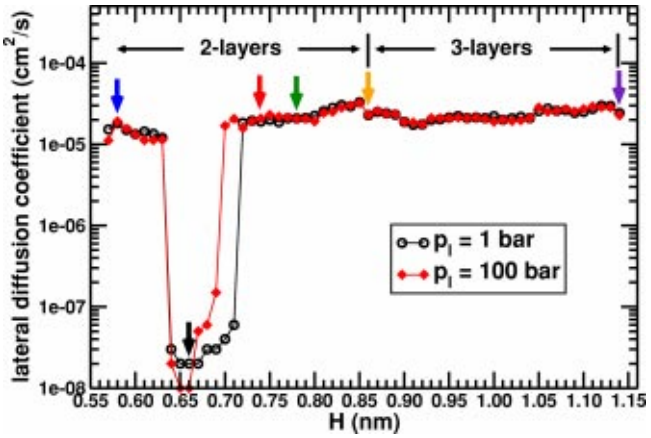

FIG. 1. In-plane diffusion coefficients of water as a function of the distance between the confining parallel plates for two values of the lateral pressure, P_l, at $T=300$ K. The arrows with different colors indicate different values of plate separations ($H=0.58$, 0.66, 0.74, 0.78, 0.86, and 1.14 nm) representing different phases and were used for further analysis in the following figures.

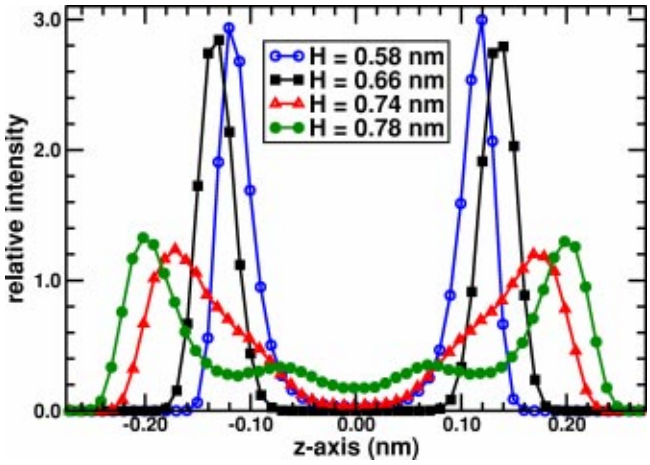

FIG. 2. Transverse density profile of oxygen atoms for different values of plate separation H representing: small-H bilayer of liquid water, HDL ($H=0.58$ nm), bilayer ice ($H=0.66$ nm), and large-H bilayer of liquid water, LDL ($H=0.74$ and 0.78 nm).

ecules changes from free diffusion to small amplitude fluctuations around fixed positions with occasional cooperative jumps. At $H=0.72$ nm for $P_l=1$ bar and at $H=0.70$ nm for $P_l=100$ bar, the frozen bilayer transforms back to a bilayer of liquid water which is stable up to $H=0.85$ nm. With further increase of the plate separation, $0.86\ \text{nm}\leqslant H\leqslant 1.13$ nm, the phase is three-layer liquid water. At $H=1.14$ nm there is a transformation to a four-layer liquid system.

The freezing of a monolayer of liquid water has been shown to be coupled to a buckling transition.[36] This is because in a monolayer arrangement the ordered out-of-plane displacement of the molecules in the buckled phase enables a reduction of the distortions in the hydrogen bonds. In the bilayer case, however, examination of the density profile of the oxygen atoms normal to the plane (for the entire range of values of H that spans its region of stability) reveals that the distribution is bimodal; one peak for each layer. The transverse density profile is shown in Fig. 2 for several specific plate separations. Nevertheless, the arrangement of oxygen atoms in the ice bilayer must allow a hydrogen bonding network with a relatively small degree of distortion from ideal geometry. The O–H–O angle profiles are shown in Fig. 3. The shape of the curve for the ice bilayer is broadened (compared to the curves of the liquid phases) and centered around an angle of 155°. The average number of hydrogen bonds per molecule for $H=0.58$, 0.74, and 0.78 nm (the liquid phases) is 3.4 and for $H=0.66$ nm (bilayer ice) is 3.8. The ratio of these numbers is represented in Fig. 3 by the size of the area under each curve.

Ab initio calculations predict the O–H–O angle in the water dimer to be anywhere between 180 and 155° (with a negligible change in energy). The fact that this angle is not far from 180° points to the validity of the localized orbital picture of an O–H bond approaching a lone pair. Although larger distortions which decrease the depth of the potential well do occur, for angles smaller than 140° there is an onset of a significant loss of energy.[38] This means that the distortion of about 155° that we find in the ice bilayer is reasonable.

Figure 4(a) displays the oxygen–oxygen radial distribution functions for various plate separations. The short–range order in the plots corresponding to $H=0.58$, 0.74, and 0.78 nm reflects the disorder of the liquid phase. However, the long-range order at $H=0.66$ nm indicates that the system has adopted a crystalline phase.

Instantaneous configurations from the MD simulations that correspond to a small-H bilayer of liquid water ($H=0.58$ nm), a bilayer ice ($H=0.66$ nm), and to a large-H bilayer of liquid water ($H=0.74$ nm) are shown in Fig. 5. The in-plane symmetry of the oxygen atoms in the ice bilayer is rhombic with a distorted in-registry arrangement between the two layers. The hydrogen positions are ordered. The out-of-plane hydrogen bond connectivity exhibits order that is built of two alternating rows of water molecules that point their hydrogens toward the oxygens present in the other layer [Fig. 5(b)]. Table I lists the different phases that were

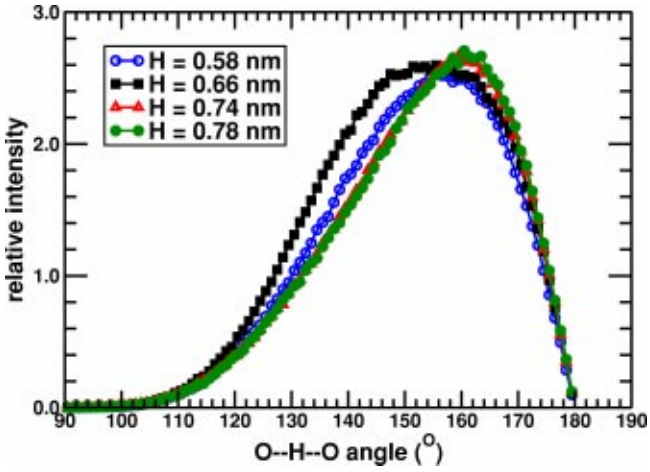

FIG. 3. Hydrogen bond angle distortion profiles. The curve for $H=0.74$ nm overlaps with the curve for $H=0.78$ nm.

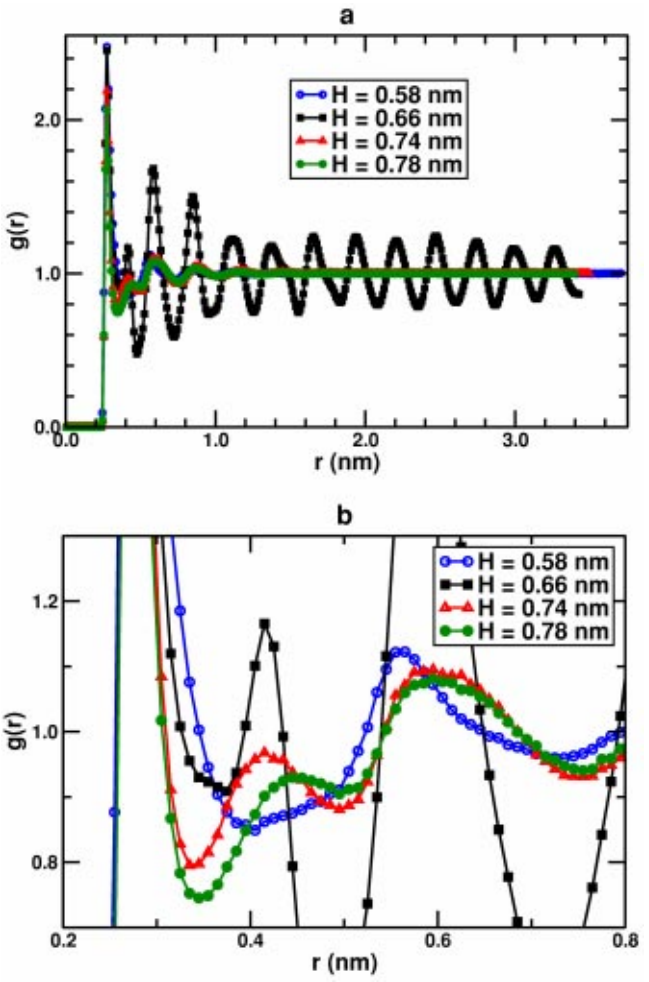

FIG. 4. (a) Radial distribution function of oxygen atoms. (b) Magnification of $g(r)$ showing the difference of the second peak between the two liquid phases.

TABLE I. The different phases observed for the simulations at $T=300$ K, $P_l=1$ bar, induced by changing H.

	H (nm)	Density (g/ml)
Small-H bilayer of liquid water (HDL)	0.57–0.63	1.11–1.02
Ice bilayer	0.64–0.71	1.05–1.01
Large-H bilayer of liquid water (LDL)	0.72–0.85	0.97–0.87
Trilayer of liquid water	0.86–1.13	1.02–0.98

observed in the simulations for plate separations in the range $0.57\ \text{nm} \leqslant H \leqslant 1.13\ \text{nm}$ with $P_l=1$ bar, along with the corresponding densities.

The abrupt change in the dynamics and in the range of structural ordering during the freezing process suggests that the transitions are first order. Simulations with temperature and lateral pressure coupling are the most appropriate to mimic experimental studies of confined system in mechanical equilibrium with the bulk; they do not allow, however, the simulation of phase coexistence. To address questions in the context of the unresolved nature of the melting in two dimensions, we investigate the order of the transition. It has been argued that two-dimensional solids lack a long-range translational order in the limit $r \to \infty$.[39–41] One of the consequences of this phenomenon is that the character of the melting transition in two dimensions can be fundamentally different from that of the melting transition in three dimensions. According to the Kosterlitz–Thouless–Halperin–Nelson–Young (KTHNY) theory,[42–46] two-dimensional solids melt via sequential continuous phase transitions. This predicts a new phase between the liquid phase and the solid phase, the so-called hexatic phase. Although, originally, the theory considers a different type of interparticle potential and a truly two-dimensional system, it is believed that this melting sce-

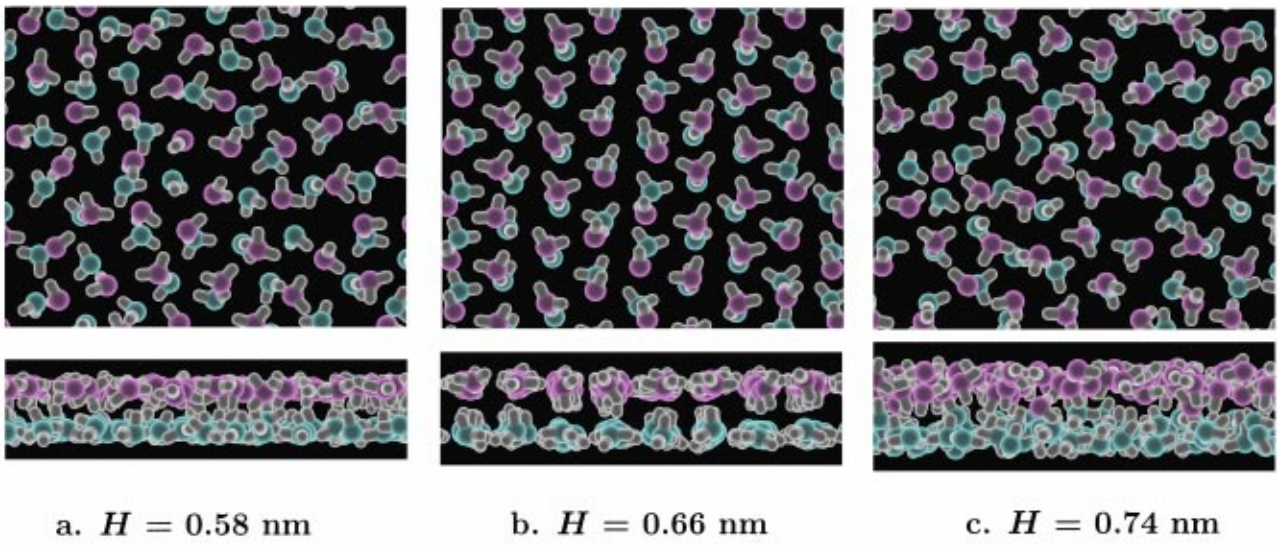

FIG. 5. In-plane and out-of-plane views showing instantaneous configurations from the MD simulations for (a) small-H bilayer of liquid water (HDL); (b) ice bilayer; and (c) large-H bilayer of liquid water (LDL). Hydrogens are depicted in white. Oxygen atoms that lie above and below the midplane along the normal axis are depicted in magenta and cyan, respectively.

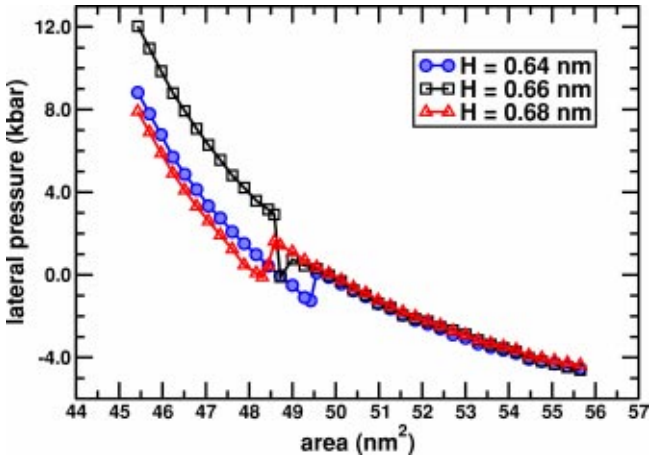

FIG. 6. Lateral pressure-area isotherms ($T=300$ K) for three values of plate separation $H=0.64$, 0.66, and 0.68 nm, indicating the first-order character of the bilayer of liquid water to bilayer ice freezing transition.

nario is universal and holds for a quasi-two-dimensional system as well.

To investigate the order of the freezing transition from a bilayer of liquid water to a bilayer of ice, a second set of the simulations was run at constant area, A, and constant H. Figure 6 shows the lateral pressure as a function of the area for three values of plate separation that support the ice bilayer. All curves have a small region showing a vdW loop shape (the reason this region is small is due to a small difference between the areal density of the bilayer of liquid water and that of the ice bilayer). The phase that exists for values of A larger than those at the transition (the region where the curves overlap) is a bilayer of liquid water, while the phase for values of A smaller than those at the transition is an ice bilayer. The results obtained from these compressibility isotherms plots indicate that the freezing transition is first order. The KTHNY scenario is probably preempted by a mechanism similar to that found in three dimensions.

In the coexistence region (the vdW loop) we did not find a clear phase separation, in contrast to the situation when a monolayer of liquid water freezes to a monolayer ice.[36] This is probably due to the small difference in the potential energy between the two phases (bilayer of liquid water and a bilayer ice), as can be inferred from the small difference in the average number of hydrogen bonds per molecule, that is insufficient to overcome the free-energy cost (loss of entropy) needed for phase separation.

The value of the lateral pressure for a fixed value of A in the region of the ice bilayer is maximal for $H=0.66$ nm. This is a manifestation of the system achieving an optimal value of plate separation for which the structure of the ice bilayer allows the distance of the hydrogen bonds to match the minimum of the interparticle potential. Such behavior would result in elastic properties that exhibit a maximum as a function of H.

The second peak in the radial distribution function at around $r=0.41$ nm for $H=0.66$ and 0.74 nm is due to the second shell of nearest-neighbor oxygen atoms in a rhombic arrangement (with angles of $\sim 100°$ and 80°) that is present in a single plane [Fig. 4(b)]. In contrast to this maximum in the $g(r)$ for $H=0.66$ and 0.74 nm (ice bilayer and LDL,

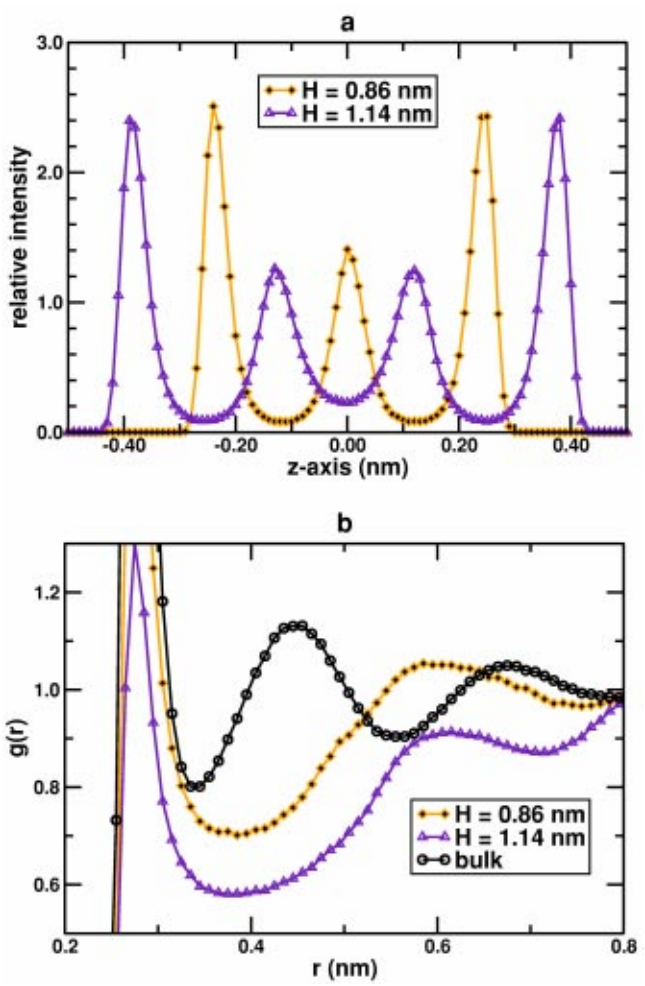

FIG. 7. (a) Transverse density profile of oxygen atoms for water confined to three layers ($H=0.86$ nm) and to four layers ($H=1.14$ nm). These values of H correspond to points where the system has just transformed (approaching the transition plate separation from below) to the specified number of layers. (b) Radial distribution functions of the oxygen atoms showing the similarities of the positions of the second peak for $H=0.86$ and 1.14 nm to that of $H=0.58$ nm shown in Fig. 4(b). The pair distribution of bulk TIP5P is also shown for comparison.

respectively), the radial distribution function for $H=0.58$ nm (HDL) at $r=0.41$ nm exhibits a minimum. Hence, the liquid phase that exists for values of H above the region that supports freezing has a local ordering similar to that of the ice bilayer, whereas the liquid phase that exists for values of H below that required for freezing has a different local order. Upon increasing H, the large-H bilayer of liquid water (LDL) exhibits a shift of the second peak of the oxygen–oxygen radial distribution function toward larger values of r, as is shown for the case of $H=0.78$ nm. A transition to a trilayer and to four layers of liquid water occurs at $H=0.86$ nm and at $H=1.14$ nm, respectively. Figure 7 shows the transverse density profile and the radial distribution function of oxygen atoms for $H=0.86$ and 1.14 nm. At these points the oxygen–oxygen radial distribution function is similar to that for the small-H bilayer of liquid water (HDL) shown for $H=0.58$ nm in Fig. 4(b). This is probably due to the fact that when the value of H is just enough to allow a transformation to a larger number of layers the arrangement of the water molecules with respect to each other has to be

modified due to the spatial constraints, and the resulting liquid phase has a higher density.

Despite the behavior of the radial distribution function, the transverse density profile of the small-H bilayer of liquid water (HDL) is similar to that of the ice bilayer, while the transverse density profile of the large-H bilayer of liquid water (LDL) exhibits a splitting of each of the layers. This is shown in Fig. 2 for $H=0.74$ and 0.78 nm (for $H=0.74$ nm the splitting is evident only as ''shoulders'' on the main peaks). The ratio between the intensity of the peaks is very similar to those of confined solids corresponding to a two-layered buckled phase.[47–49] However, in the liquid phase there is an overlap between the peaks resulting from diffusion of particles between the different planes.

The peaks of the transverse density profile representing different layers are always split in two in the buckled phase. These phases, that occur in spatially inhomogeneous systems, are regarded as intermediate phases that interpolate between structures with integral number of layers. The transformation to a larger number of layers as H is increased is performed by the merging of peaks that originate from different layers.[49,50] Consider the bilayer case, where the transverse density profiles for $H=0.74$ and 0.78 nm are shown in Fig. 2. Each layer is split in two, with relative magnitudes of approximately 2/3 and 1/3 for the peak that is closer to the wall and for the peak that is closer to the center, respectively. As H increases the two peaks with the relative magnitude of 1/3 from different layers (at around $z=\pm 0.08$ nm) approach each other (toward $z=0$) and finally merge to form a three-layer system where each peak has an equal relative intensity of 2/3. The transverse density profile of a trilayer of liquid water is shown in Fig. 7(a).

The difference in the structure of the two liquid phases was reproduced upon melting of the ice bilayer, induced by decreasing H. Note that the effect of higher lateral pressure in the first set of simulations is to destabilize the ice bilayer as is shown in Fig. 1; the ice bilayer transform to the liquid phase at $H=0.72$ nm for $P_l=1$ bar while it transforms at $H=0.70$ nm for $P_l=100$ bar. Although a thermodynamic characterization of the liquid–liquid transition is not given in this study, it is likely that at higher temperature or at higher lateral pressure, where the ice bilayer becomes unstable with respect to either of the liquid phases, a direct transition between the two liquid phases would be possible.

Liquid–liquid phase transitions have been reported for confined water between a bilayer liquid with a split normal density profile and a trilayer liquid water.[16] The large-H bilayer of liquid water (LDL) that we find is this study has a second peak at approximately the same location as the one reported by Meyer and Stanley obtained with Monte Carlo simulations with the ST2 model potential for water.[16] It also qualitatively resembles the one reported by Bosio and co-workers obtained from x-ray and neutron scattering experiments of water confined in pores of poly(2-hydroxyethylmethacrylate)[26] and at a hydrophobic surface.[27] These studies conclude that the molecular structure of water under an environment that disrupts its ability to establish a tetrahedral network of nearest neighbors exhibits a distortion at the second neighbor level. In these cases, a hump at around $r=0.37$ nm is observed while the packing of the first neighbors is not significantly affected.

The observation of sequential freezing and melting transitions as H is increased is similar to the behavior of water confined to a monolayer.[36] Experimental support for such a phenomenon comes from studies using a mercury/water/mercury tunnel junction at $T=265$ K, where it was found that the Young's modulus of two-dimensional ice shows a maximum value (of $\sim 20\%$ of bulk ice I_h) as H was increased from 0.50 to 0.80 nm.[51] Particles under confinement exhibit large oscillations in the density as a function of H that span transitions between consecutive number of layers. Since the ordinary ice, I_h, is sensitive to density (e.g., melting can be observed upon increasing the density), the alternation of water and ice phases as a function of H in confined geometries can be understood in these terms. However, since the space is inhomogeneous and is divided into lateral and transverse subspaces, the density itself does not serve as a suitable thermodynamic variable.

Figure 1 also indicates that no freezing transition occurs at any value of plate separation for water confined to three layers at $T=300$ K and at ambient pressures. Further simulations of water at the same conditions confined to $4-8$ layers ($1.15\ \text{nm} \leqslant H \leqslant 2.56\ \text{nm}$) also indicate that water remains in the liquid phase (the lateral diffusion coefficient was found to be in the range $2-3\times 10^{-5}$ cm^2/s), which is comparable to the diffusion coefficient of the bulk. This means that above the film thickness of a bilayer, the degree to which the solid phase is stabilized due to confinement is insufficient to freeze liquid water at ambient conditions. These findings are consistent with experimental measurements of the effective viscosity of water confined between mica surfaces[52] and can be attributed to the incompatibility between the tetrahedral arrangement of water and a slab geometry.

ACKNOWLEDGMENTS

This research has been supported by a Marie Curie Fellowship of the European Community, the Fifth Framework Program, under Contract Number MCFI-1999-00161 and by the Soft-Link project under Project Number 98SL010.

[1] C. L. Rhykerd, M. Schoen, D. J. Diestler, and J. H. Cushman, Nature (London) **330**, 461 (1987).
[2] J. N. Israelachvili, P. M. McGuiggan, and A. M. Homola, Science **240**, 189 (1988).
[3] M. L. Gee, P. M. McGuiggan, J. N. Israelachvili, and A. M. Homola, J. Chem. Phys. **93**, 1895 (1990).
[4] S. Granick, Science **253**, 1374 (1991).
[5] J. E. Hug, F. van Swol, and C. F. Zukoski, Langmuir **11**, 111 (1995).
[6] J. Klein and E. Kumacheva, Science **269**, 816 (1995).
[7] J. Gao, W. D. Luedtke, and U. Landman, Phys. Rev. Lett. **79**, 705 (1997).
[8] J. Klein and E. Kumacheva, J. Chem. Phys. **108**, 6996 (1998).
[9] S. T. Cui, P. T. Cummings, and H. D. Cochran, J. Chem. Phys. **114**, 7189 (2001).
[10] M. Antognozzi, A. D. L. Humphris, and M. J. Miles, Appl. Phys. Lett. **78**, 300 (2001).
[11] H. E. Stanley *et al.*, Physica A **306**, 230 (2002).
[12] P. H. Poole, F. Sciortino, U. Essmann, and H. E. Stanley, Nature (London) **360**, 324 (1992).
[13] M. Yamada, S. Mossa, H. E. Stanley, and F. Sciortino, Phys. Rev. Lett. **88**, 195701 (2002).
[14] I. Brovchenko, A. Geiger, and A. Oleinikova, J. Chem. Phys. **118**, 9473 (2003).

[15] Y. Katayama *et al.*, Nature (London) **403**, 170 (2000).
[16] M. Meyer and H. E. Stanley, J. Phys. Chem. B **103**, 9728 (1999).
[17] I. Brovchenko, D. Paschek, and A. Geiger, J. Chem. Phys. **113**, 5026 (2000).
[18] P. Gallo, M. Rovere, and E. Spohr, J. Chem. Phys. **113**, 11324 (2000).
[19] I. Brovchenko and A. Geiger, J. Mol. Liq. **96–97**, 195 (2002).
[20] P. Gallo, M. Rapinesi, and M. Rovere, J. Chem. Phys. **117**, 369 (2002).
[21] K. Koga, X. C. Zeng, and H. Tanaka, Phys. Rev. Lett. **79**, 5262 (1997).
[22] J. Slovak, H. Tanaka, K. Koga, and X. C. Zeng, Physica A **319**, 163 (2003).
[23] B. Kamb, ''Crystallography of ice,'' in *Physics and Chemistry of Ice*, edited by E. Whalley, S. J. Jones, and L. W. Gold (Royal Society of Canada, Ottawa, 1973), pp. 28–41.
[24] E. Whalley, ''The hydrogen bond in ice,'' in *The Hydrogen Bond*, edited by P. Schuster, G. Zundel, and C. Sandorfy (North-Holland, Amsterdam, 1976), pp. 1427–1470.
[25] Y. E. Gorbaty and Y. N. Demianets, Mol. Phys. **55**, 571 (1985).
[26] L. Bosio, G. P. Johari, M. Oumezzine, and J. Teixeira, Chem. Phys. Lett. **188**, 113 (1992).
[27] M.-C. Bellissent-Funel, R. Sridi-Dorbez, and L. Bosio, J. Chem. Phys. **104**, 10023 (1996).
[28] E. Lindal, B. Hess, and D. van der Spoel, J. Mol. Model. [Electronic Publication] **7**, 306 (2001).
[29] H. J. C. Berendsen, J. P. M. Postma, W. F. van Gunsteren, A. DiNola, and J. R. Haak, J. Chem. Phys. **81**, 3684 (1984).
[30] I. G. Tironi, R. Sperb, P. E. Smith, and W. F. van Gunsteren, J. Chem. Phys. **102**, 5451 (1995).
[31] M. W. Mahoney and W. L. Jorgensen, J. Chem. Phys. **112**, 8910 (2000).
[32] W. F. van Gunsteren *et al.*, *Biomolecular Simulation*: GROMOS96 *Manual and User Guide* (BIOMOS b.v., Zürich, Groningen, 1996).
[33] A. Bondi, J. Phys. Chem. **68**, 441 (1964).
[34] S. Miyamoto and P. A. Kollman, J. Comput. Chem. **13**, 952 (1992).
[35] H. J. C. Berendsen and W. F. van Gunsteren, ''Molecular dynamics simulations: Techniques and approaches,'' in *Molecular Liquids—Dynamics and Interactions*, edited by A. J. Barnes *et al.*, NATO ASI C 135 (Reidel, Dordrecht, 1984), pp. 475–500.
[36] R. Zangi and A. E. Mark, Phys. Rev. Lett. (to be published).
[37] M. W. Mahoney and W. L. Jorgensen, J. Chem. Phys. **114**, 363 (2001).
[38] C. N. R. Rao, ''Theory of hydrogen bonding in water,'' in *Water: A Comprehensive Treatise*, edited by F. Franks (Plenum, New York, 1972), pp. 93–149.
[39] N. D. Mermin, Phys. Rev. **176**, 250 (1968).
[40] R. Peierls, *Surprises in Theoretical Physics* (Princeton University Press, Princeton, NJ, 1979).
[41] L. Landau and E. Lifshitz, *Statistical Physics* (Pergamon, Oxford, 1986).
[42] J. M. Kosterlitz and D. J. Thouless, J. Phys. C **5**, L124 (1972).
[43] J. M. Kosterlitz and D. J. Thouless, J. Phys. C **6**, 1181 (1973).
[44] B. I. Halperin and D. R. Nelson, Phys. Rev. Lett. **41**, 121 (1978).
[45] D. R. Nelson and B. I. Halperin, Phys. Rev. B **19**, 2457 (1979).
[46] A. P. Young, Phys. Rev. B **19**, 1855 (1979).
[47] S. Neser, C. Bechinger, P. Leiderer, and T. Palberg, Phys. Rev. Lett. **79**, 2348 (1997).
[48] R. Zangi and S. A. Rice, Phys. Rev. E **58**, 7529 (1998).
[49] R. Zangi and S. A. Rice, Phys. Rev. E **61**, 660 (2000).
[50] M. Schmidt and H. Löwen, Phys. Rev. E **55**, 7228 (1997).
[51] J. D. Porter and A. S. Zinn-Warner, Phys. Rev. Lett. **73**, 2879 (1994).
[52] U. Raviv, P. Laurat, and J. Klein, Nature (London) **413**, 51 (2001).